Heliyon 10 (2024) e29360

Contents lists available at ScienceDirect

Heliyon

journal homepage: www.cell.com/heliyon

Research article

Mechanism of Danggui Buxue decoction in the treatment of myocardial infarction based on network pharmacology and experimental identification

Chuqiao Shen [a], Qian Chen [b], Shuo Chen [b], Yixuan Lin [c,*]

[a] Department of Pharmacy, The First Affiliated Hospital of Anhui University of Chinese Medicine, Hefei, Anhui, 230031, China
[b] Key Laboratory of Xin'an Medicine, Ministry of Education, Anhui Province Key Laboratory of R&D of Traditional Chinese Medicine, Anhui University of Chinese Medicine, Hefei, Anhui, 230038, China
[c] Department of Endocrinology, The First Affiliated Hospital of Anhui University of Chinese Medicine, Hefei, Anhui, 230031, China

ARTICLE INFO

Keywords:
Danggui buxue decoction
Myocardial infarction
Network pharmacology
Molecular docking
PI3K/AKT1

ABSTRACT

Background: Myocardial infarction (MI) remains one of the major causes of high morbidity and mortality worldwide. Danggui Buxue Decoction (DBD)—an ancient Chinese herbal decoction—has been used to prevent coronary heart disease, which was called "chest palsy" in ancient clinics. However, the mechanism of DBD in the treatment of MI remains unclear. The aim of this study was to explore the effect and mechanism of DBD on MI by combining network pharmacology with *in vivo* experiments.

Materials and methods: First, public databases were used to identify the key active chemicals and possible targets of DBD. The MI targets were obtained from the Therapeutic Target Database, and the function of the target genes in relation to linked pathways was investigated. **Subsequently,** Cytoscape software was used to build a target-signaling pathway network. Finally, the efficacy of DBD therapy on MI was validated using *in vivo* investigations combined with molecular docking.

Results: In traditional Chinese medicine systems pharmacology database and analysis platform (TCMSP), 27 bioactive compounds were screened from DBD. A total of 213 common targets were obtained, including 507 DBD targets and 2566 MI targets. Enrichment analysis suggests that PI3K/AKT is a potential signaling pathway for DBD-based protection. Immunofluorescence and protein blotting confirmed PI3K/AKT1, ERK2, and CASPASE-9 as the target proteins. Molecular docking analysis showed that quercetin, kaempferol, isoflavanones, isorhamnetin, hederagenin, and formononetin had high binding affinity to AKT1, ERK2, and CASPASE-9.

Conclusions: This study demonstrated that the therapeutic benefit of DBD on MI may be mediated via target proteins in the PI3K/AKT pathway, such as AKT1, ERK2, and CASPASE-9. Our study data can help to provide ideas and identify new treatment targets for MI.

1. Introduction

Cardiovascular diseases (CVDs) have high global incidence and are a serious threat to human health with high rates of mortality [1,

* Corresponding author.
E-mail addresses: 1535782800@qq.com (C. Shen), cq15527004210@163.com (Q. Chen), chasemoon@aliyun.com (S. Chen), 739093358@qq.com (Y. Lin).

https://doi.org/10.1016/j.heliyon.2024.e29360
Received 26 December 2023; Received in revised form 3 April 2024; Accepted 7 April 2024
Available online 9 April 2024

Abbreviations

MI	Myocardial infarction
DBD	Danggui Buxue Decoction
CVDs	Cardiovascular diseases
TCM	traditional Chinese medicine
AR	Roots of Astragalus membranaceus (Fisch.) Bunge var. mongholicus (Bunge) Hsiao
ASR	Angelica sinensis (Oliv.) Diel
TCMSP	traditional Chinese medicine systems pharmacology database and analysis platform
OB	oral bioavailability
DL	drug-likeness
OMIM	Online Mendelian Inheritance in Man
TTD	Therapeutic Target Database
GO	Gene Ontology
KEGG	Kyoto Encyclopedia of Genes and Genomes
BP	biological process
CC	cellular component
MF	molecular function
LAD	left anterior descending
TTC	2,3,5-Triphenyltetrazolium Chloride
H&E	hematoxylin and eosin

2]. Myocardial infarction (MI) is one of the most acute forms of ischemic heart disease, and refers to the necrosis of any size of myocardial cells induced by myocardial ischemia. MI-related morbidity has declined in recent years owing to widespread use of thrombolysis, cardiac interventional surgery, and drug discovery, but the mortality rate remains high. Treatment with creatine phosphate and ubidecarenone has short-term effects on improving the energy process in contraction, while beta-receptor blockers and calcium antagonists are used to relieve chronic coronary syndrome. Several studies have found that traditional Chinese medicine (TCM) has obvious advantages in the treatment of MI [3–5].

Danggui Buxue Decoction (DBD), composed of Astragali Radix [AR; roots of *Astragalus membranaceus* (Fisch). Bunge or *A. membranaceus* (Fisch). Bunge var. *mongholicus* (Bunge) Hsiao] and Angelicae Sinensis Radix [ASR; roots of *Angelica sinensis* (Oliv.) Diels] was recorded in "Neiwaishang Bianhuo lun" by Li Dongyuan in the Jin dynasty (about AD 1247), and was at a ratio of 5:1 [6,7]. To date, DBD has been found to have various clinical benefits that are useful in cardioprotection [8,9] and amelioration of blood deficiency [10–12]. In addition, laboratory studies have found that DBD has anti-oxidative [13], anti-myocardial fibrosis [14], anti-inflammatory [15], and immune regulatory properties [16]. According to TCM, DBD can be used to prevent cardiovascular and circulatory diseases based on "Xing Qi Huo Xue" and treat MI. However, the correlation between the active chemicals in DBD and the underlying mechanisms has not yet been clarified, which has hindered the public acceptance of TCM.

Network pharmacology is a relatively new science that is based on systems biology and has a multi-directional approach. It uses data analysis software and biological algorithms to carry out drug molecular design and target analysis, as well as anticipate drug pharmacological mechanisms [17,18]. The network pharmacology technique has been frequently employed in TCM, which is consistent with the latter's holistic idea as well as syndrome differentiation and therapy [19]. Molecular docking plays an important role in predicting the binding affinity between novel drugs and peptides or proteins [20–22]. In addition, molecular docking can be performed to validate the binding ability of compounds to target proteins [23–25]. Therefore, in this study, we evaluated the underlying mechanism of DBD on MI through network pharmacology-based methods and further confirmed this mechanism by molecular docking studies to identify core target genes. We also established an *in vivo* model for experimental validation of the predicted core targets to verify the reliability of the network pharmacology methodology.

2. Materials and methods

2.1. Analysis of DBD by network pharmacology

2.1.1. Candidate compound screening

Drugs are often administered orally in clinical treatment. Therefore, we used the keywords "Radix Astragali" and "Radix Angelicae Sinensis" to screen the active ingredients and targets in the Traditional Chinese Medicine Systems Pharmacology Database and Analysis Platform (TCMSP, http://tcmspw.com/tcmsp.php) [25]. Previous research found that ferulic acid, ligustilide, Astragaloside (AS)-II, AS-III, AS-IV, and calycosin-7-O-D-glucoside added on the screening list [14,26].

2.1.2. Potential MI targets of DBD

The MI-related gene targets were collected by searching the keywords "MI" from four databases, namely GeneCards (database of human genes, https://www.genecards.org/, v5.3.0) [27]; Online Mendelian Inheritance in Man (OMIM, http://www.omim.org/,

updated June 26, 2021) [28]; Therapeutic Target Database (TTD, http://db.idrblab.net/ttd/, updated June 1, 2020); and Drugbank database (https://go.drugbank.com/, version 5.1.8). All corresponding targets for each potential active compound were collected from the TCMSP and matched using the SwissTargetPrediction (http://www.swisstargetprediction.ch/) database with a high probability (score>0.1) included in the results [29]. Then, these targets were normalized in Uniprot (https://www.uniprot.org/) [30]. Subsequently, we drew a Venn diagram using Draw Venn Diagram (http://bioinformatics.psb.ugent.be/webtools/Venn/) to summarize the intersections between DBD and MI.

2.1.3. Construction of drug-component-target-disease network

The topology network of DBD compounds in correlation with gene targets was used to collect the most active chemical components in response to MI treatment. This was analyzed using Cytoscape software (version 3.8.2; https://www.cytoscape.org/) [31], which quantified the degree of each node and made nodes with higher degree values larger. A greater number of edges for the compound nodes corresponded to a higher activity level.

2.1.4. Screening of action targets and construction of protein–protein interaction (PPI) network

The PPI network was built using the STRING protein interaction analysis platform (Search Tool for the Retrieval of Interacting Genes 11.0) database (https://string-db.org/) [32] by importing the overlapping gene targets of DBD and MI and specifying the species as "Homo sapiens" with a cut-off confidence score of $\geq$0.9. Furthermore, we utilized Cytoscape's CytoHubba plugin to present the PPI network picture, with deeper-colored nodes signifying higher scores [33]. To select core genes in the network, the top overlapping genes among significant topological parameters such as Degree, Betweenness, Closeness, and Maximal Clique Centrality (MCC) were analyzed. In addition, the Molecular Complex Detection (MCODE) plugin was based on the topology to identify densely connected regions in the PPI network, with a higher score indicating greater correlation of the nodes [34].

2.1.5. Pathway and functional enrichment analysis

The Gene Ontology (GO) [35] and Kyoto Encyclopedia of Genes and Genomes (KEGG) pathway enrichment analysis [36] were considered statistically significant to screen out the potential signaling pathway associated with the mechanism of action of DBD against MI. The GO terms including biological process (BP), cellular component (CC), and molecular function (MF) together with KEGG were performed using the Functional Annotation Tool in DAVID and Metascape, with $P < 0.05$ as the screening criterion.

2.1.6. Molecular docking validation

Molecular docking is frequently performed in drug discovery studies owing to its capacity to shed light on the mechanism of bindings between the target proteins and drug molecular ligands [37]. All molecular compound 2D structure SDF files were derived from the PubChem database (https://pubchem.ncbi.nlm.nih.gov/). In addition, PDB format of the core targets was downloaded from the RCSB database (http://www.rcsb.org/). CB-Dock software (http://clab.labshare.cn/cb-dock/php/) was used for molecular docking, and the binding ability between ligand and receptor was evaluated according to the Vina score [38].

2.2. Experimental validation

2.2.1. Reagents and materials

Roots of *Astragalus membranaceus* (Fisch.) Bunge var. *mongholicus* (Bunge) Hsiao (AR) and *Angelica sinensis* (Oliv.) Diel (ASR) (Batch 2011060081) were purchased from Huqiaogroup Co., Ltd. (Bozhou, China). Primary antibodies against AKT1 (AF0836) and CASPASE-9 (AF6348) were purchased from Affinity Biosciences (OH, USA), and primary ERK2 (GB11370) antibody and hematoxylin-eosin (H&E) stain were purchased from Servicebio (Wuhan, China). 2,3,5-triphenyltetrazolium chloride (TTC) (T8877) was purchased from Sigma-Aldrich (Ca, USA).

2.2.2. Preparation of DBD

DBD was prepared using a water decoction as described previously. AR (500 g) and ASR (100 g) were weighed and soaked in 8-times the volume of purified water for 90 min at room temperature, brought to a boil, and simmered for 60 min. The herbs were extracted twice. Finally, the liquid obtained from the two decoctions was mixed and concentrated to 1 L using a rotary evaporator.

2.2.3. Analysis of DBD by ultra-performance liquid chromatography (UPLC)

Waters Acquity UPLC H-Class system (Waters, Milford, MA) was used to identify the major components of DBD in a qualitative manner. The Acquity BEH C18 column has dimensions of 2.1 mm $\times$ 100 mm and 1.7 μm. The mobile phase was a 0.05 % (v/v) phosphoric acid-distilled water (A) and acetonitrile (B) system, with gradient elution of 5–15 % B for 0–2 min, 15–90 % B for 2–10 min, 90–90 % B for 10–11 min, and 90–5% B for 11–12 min. The column temperature, flow rate, injection volume, and wavelength were set to 30 °C, 0.2 mL/min, 1 μL, and 280 nm, respectively.

2.2.4. Animal experiments

All animal experiments were carried out following the EEC Directive of 1986 (86/609/EEC) and were approved by the Ethics Committee of the Anhui University of Chinese Medicine (AHUCM-rats-2022008). Adult male Sprague–Dawley rats (180−220 g at 6–7 weeks) were purchased from Hangzhou Ziyuan Experimental Animal Technology Co., Ltd. (Hangzhou, China, Laboratory Animal Production; License No. SCXK [Zhejiang] 2019-0004). Rats were housed at room temperature (25 $\pm$ 2 °C) with *ad libitum* access to food

and water. Light control, and underwent adaptive feeding for 1 week for habituation.

2.2.5. Model preparation and administration

After 7 days of adoption, all rats were randomly assigned to three groups (n = 6 per group), as shown in Fig. 1: (1) sham group; (2) MI group; (3) MI + DBD group. Rats in the MI + DBD group were administered 10 g/kg/d DBD (according to clinical dosage conversion) by the intragastric route for one week before MI surgery, while rats in the other two groups received equal amounts of saline. To avoid intestinal obstruction, rats were fasted for 12 h before the surgery. To establish the MI model, all rats were anesthetized with 1 % pentobarbital (40 mg/kg) and placed supine on the console. After intubation with a small-animal ventilator (R415, RWD Life Science Co., Ltd., Shenzhen, China), MI was simulated in the rats by using the method of closure of the left anterior descending (LAD) coronary artery with a 6-0 polypropylene suture at a position ~2–3 mm from the lower edge of the left auricle. Subsequently, the heart was placed back into the chest cavity, followed by skin suturing. Electrocardiogram monitoring was performed immediately to verify the success of MI surgery: T wave variation and ST-segment elevation. LAD ligation was not performed and similar operations were performed on the sham rats. Finally, all rats were intraperitoneally injected with 1 % sodium pentobarbital (150 mg/kg) to collect the heart samples; the heart was excised and stored at −80 °C until further analysis.

2.2.6. Infarct area measurement

Whole rat heart was collected and rinsed with cold normal saline, and stored at −80 °C for 15 min until frozen, followed by cutting into five sections with 1 mm thickness. Then, the slices were placed in 1 % 2,3,5-Triphenyltetrazolium Chloride (TTC) solution in a 37 °C water bath for 20 min, followed by steeping in 10 % neutralized formalin for 4 h. After washing with distilled water, the heart slices were fixed in paraformaldehyde, and visualized using a Canon digital camera. The infarct area (either unstained or faintly stained) and the non-infarct left ventricle area (stained red) were calculated using Image J (1.53e) software (https://imagej.net/ij/).

2.2.7. Histological analysis

Freshly treated heart tissues in 4 % paraformaldehyde were embedded in paraffin. H&E staining of the left ventricle tissue slices (5 μM) was followed by washing to examine the histoarchitectural changes. Following dehydration and sealing, the slices were examined and photographed using optical microscopy. The black arrow represents the invasion of inflammatory cells.

2.2.8. Western blotting validation assay

Proteins from cardiac tissue were separated using SDS-PAGE before being transferred to a polyvinylidene fluoride (PVDF) membrane and blocked with 5 % skimmed milk. The PVDF membrane was then incubated for 24 h at 4 °C with primary antibodies against AKT1 (1:1000), ERK2 (1:1000), CASPASE-9 (1:1000), and β-Actin (1:1000), followed by secondary antibody incubation (1:20000; Abbkine, Wuhan, China). The proteins were then monitored and evaluated with Image J (1.53e) upon enhanced chemiluminescence detection.

2.2.9. Immunofluorescence validation assay

Heart tissue sections were sliced, followed by antigen repair in the microwave, and then blocked and incubated with rabbit

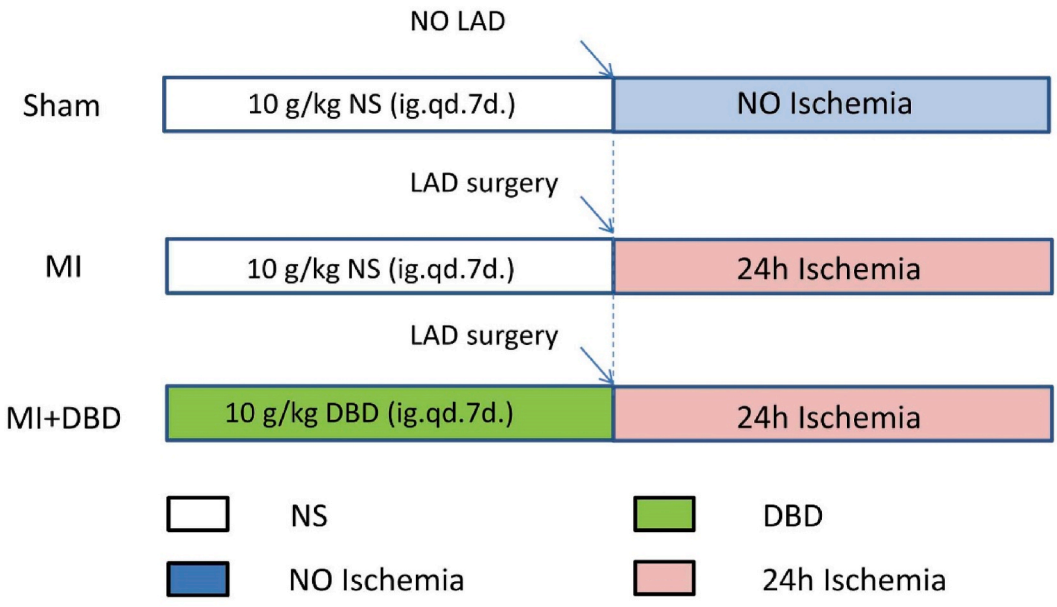

Fig. 1. Diagram of the ischemic rat heart model treated with DBD.

polyclonal antibodies (1:2000) against AKT1, ERK2, and CASPASE-9 overnight at 4 °C. The sections were washed with 0.01 M TBS (pH 7.4) several times and incubated at 37 °C with tetramethylrhodamine isothiocyanate (TRITC)-conjugated goat anti-rabbit IgG for 50 min. After washing with PBS, the sections were incubated with DAPI solution for 10 min at 37 °C to stain the nuclei. Finally, the slides were imaged using a NIKON ECLIPSE C1 microscope, and immunofluorescence was analyzed using Image J (1.53e) software.

2.2.10. Terminal deoxynucleotidyl transferase dUTP nick-end labeling (TUNEL) validation for myocardial apoptosis assay

Myocardial apoptosis was detected by TUNEL staining with 3,3-diaminobenzidine (DAB). Briefly, the heart sections were prepared with TUNEL detection solution (TdT enzyme 5 μL and Biotin-dUTP 45 μL). Then, 50 μL TUNEL detection solution was added to the sample and incubated at 37 °C for 60 min. Next, 50 μL streptavidin-HRP working solution was added dropwise and incubated at room temperature for 30 min. Samples were incubated with DAB at room temperature for 5–30 min, and hematoxylin staining of nuclei was performed. The cardiomyocyte apoptosis was measured under a Nikon eclipse 50i microscope. The normal cells' nuclei were stained blue, and the TUNEL-positive cardiomyocytes were stained brown (black arrow).

2.2.11. Statistical analysis

Statistical analysis was performed using GraphPad Prism 9.0 software, with mean ± standard deviation (x±SD) for independent samples, *t*-test for group comparisons, and one-way analysis of variance for multiple group comparisons $^{**}p < 0.01$ and $p < 0.05$ indicated a statistically significant difference. Differential analysis of GO terms and KEGG pathway enrichment was analyzed by using Metascape software, and results were considered statistically significant at $p < 0.01$.

3. Results

3.1. Network pharmacology-based analysis

3.1.1. Potential active ingredients in DBD

In TCMSP, 27 potentially active ingredients of DBD were screened, including 23 ingredients from AR and four ingredients from ASR (compound details are shown in Table 1). Then, 508 target genes of potential active compounds were identified in the databases (TSMSP and Swiss Target Prediction). In addition, after removing 27 targets with a reliability of 0 and duplicates, we identified 2566 MI targets genes from the databases (GeneCards, OMIM, and TTD). Finally, 213 overlapping common protein targets between DBD and MI were obtained through intersection (Fig. 2A).

3.1.2. DBD active ingredient-target network diagram

After inputting the DBD active ingredients and potential targets into Cytoscape 3.8.2, the DBD active ingredient-target network

Table 1
Detailed information of the 27 active compounds from DBD.

No.	Compound Name	MOL ID	OB (%)	DL	Herb
1	Mairin	MOL000211	55.38	0.78	AR
2	Jaranol	MOL000239	50.83	0.29	AR
3	hederagenin	MOL000551	36.91	0.75	AR
4	(3S,8S,9S,10R,13R,14S,17R)-10,13-dimethyl-17-[(2R,5S)-5-propan-2-yloctan-2-yl]-2,3,4,7,8,9,11,12,14,15,16,17-dodecahydro-1H-cyclopenta[a]phenanthren-3-ol	MOL000033	36.23	0.78	AR
5	isorhamnetin	MOL000354	49.60	0.31	AR
6	3,9-di-O-methylnissolin	MOL000371	53.74	0.48	AR
7	7-O-methylisomucronulatol	MOL000378	74.69	0.3	AR
8	9,10-dimethoxypterocarpan-3-O-β-D-glucoside	MOL000379	36.74	0.92	AR
9	(6aR,11aR)-9,10-dimethoxy-6a,11a-dihydro-6H-benzofurano[3,2-c]chromen-3-ol	MOL000380	64.26	0.42	AR
10	Bifendate	MOL000387	31.10	0.67	AR
11	Formononetin	MOL000392	69.67	0.21	AR
12	Isoflavanone	MOL000398	109.99	0.3	AR
13	Calycosin	MOL000417	47.75	0.24	AR
14	Kaempferol	MOL000422	41.88	0.24	AR
15	FA	MOL000433	68.96	0.71	AR
16	(3R)-3-(2-hydroxy-3,4-dimethoxyphenyl)chroman-7-ol	MOL000438	67.67	0.26	AR
17	isomucronulatol-7,2′-di-O-glucosiole	MOL000439	49.28	0.62	AR
18	1,7-Dihydroxy-3,9-dimethoxy pterocarpene	MOL000442	39.05	0.48	AR
19	Quercetin	MOL000098	46.43	0.28	AR
20	Astragaloside IV	MOL000407	22.50	0.15	AR
21	Calycosin-7-O-B-D-glucoside	MOL009290	47.75	0.24	AR
22	Astragaloside II	MOL000403	46.06	0.13	AR
23	Astragaloside III	MOL000405	31.84	0.10	AR
24	Beta-sitosterol	MOL008583	36.91	0.75	ASR
25	Stigmasterol	MOL000449	43.83	0.76	ASR
26	Ferulic acid	MOL000360	54.97	0.06	ASR
27	Ligustilide	MOL011782	51.30	0.07	ASR

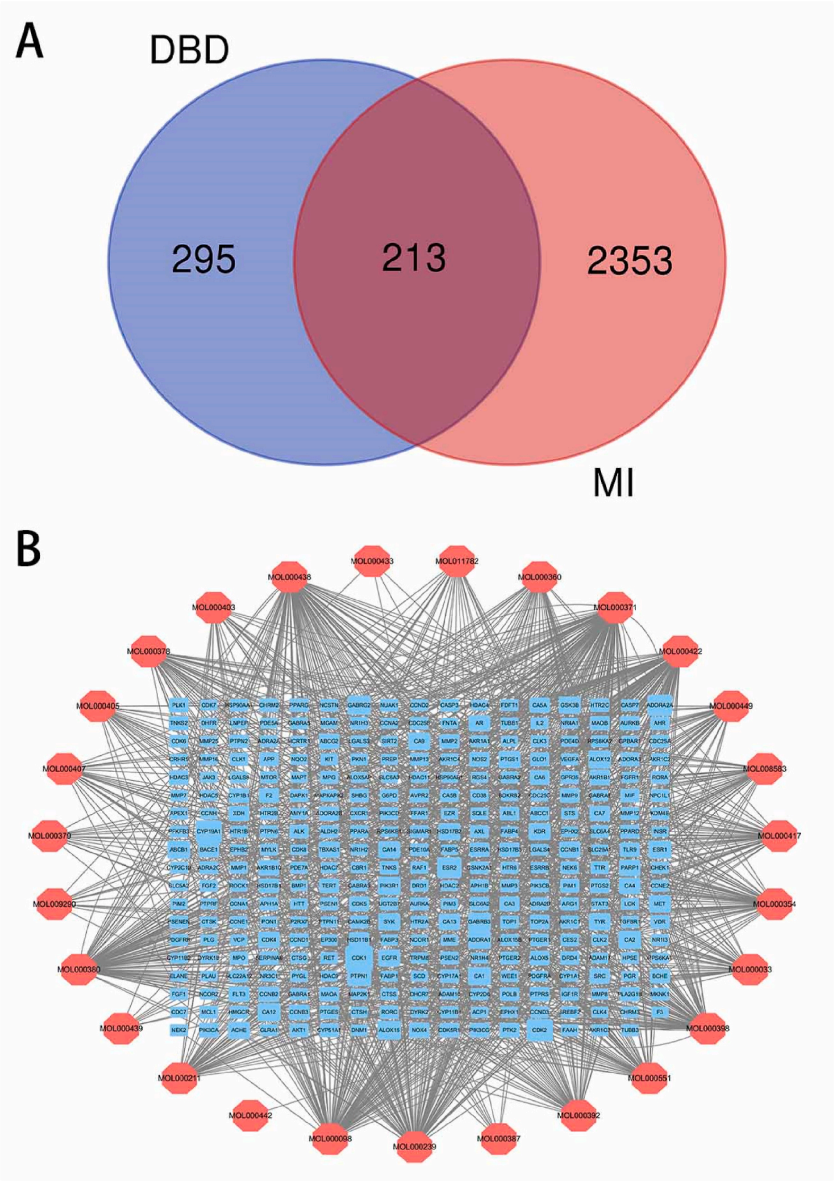

Fig. 2. Prediction from network pharmacology.
(A) Venn diagram of DBD component targets with MI targets. (B) DBD active ingredient-target network.

diagram (Fig. 2B) was drawn. There were 322 target gene nodes, 27 compound nodes, and 1366 edges in the network. The top 10 compounds information were 3,9-di-O-methylnissolin, isomucronulatol-7,2′-di-O-glucosiole, quercetin, kaempferol, (6aR, 11aR)-9,10-dimethoxy-6a, jaranol, isoflavanone, isorhamnetin, hederagenin, and formononetin. Among these compounds, quercetin [39], kaempferol [40], isoflavanone [41], isorhamnetin [40], hederagenin, and formononetin [42] were the most active compounds related to MI symptoms in DBD.

3.1.3. Hub target proteins and critical signal pathway

The STRING 11.0 database was used to construct the PPI network to identify hub target proteins, as shown in Fig. 3A. There were 213 nodes and 885 edges in the network. Furthermore, we employed the algorithms from CytoHubba to identify the top 10 proteins in 213 common targets. Table 2 displays the MCODE networks that were found for individual gene lists. Table 3 displays the top 10 proteins of Degree, Betweenness, Closeness, and MCC. Finally, we discovered the following seven key proteins by considering the intersection (Fig. 3B): PIK3R1, MAPK1, SRC, STAT3, HRAS, AKT1, and PTPN11.

To discover the key signaling pathways and biological processes, Metascape was utilized to perform enrichment analysis on the 213 effective targets for the therapy of DBD against MI. The target genes were enriched in “Pathways in cancer” (hsa05200), “Insulin

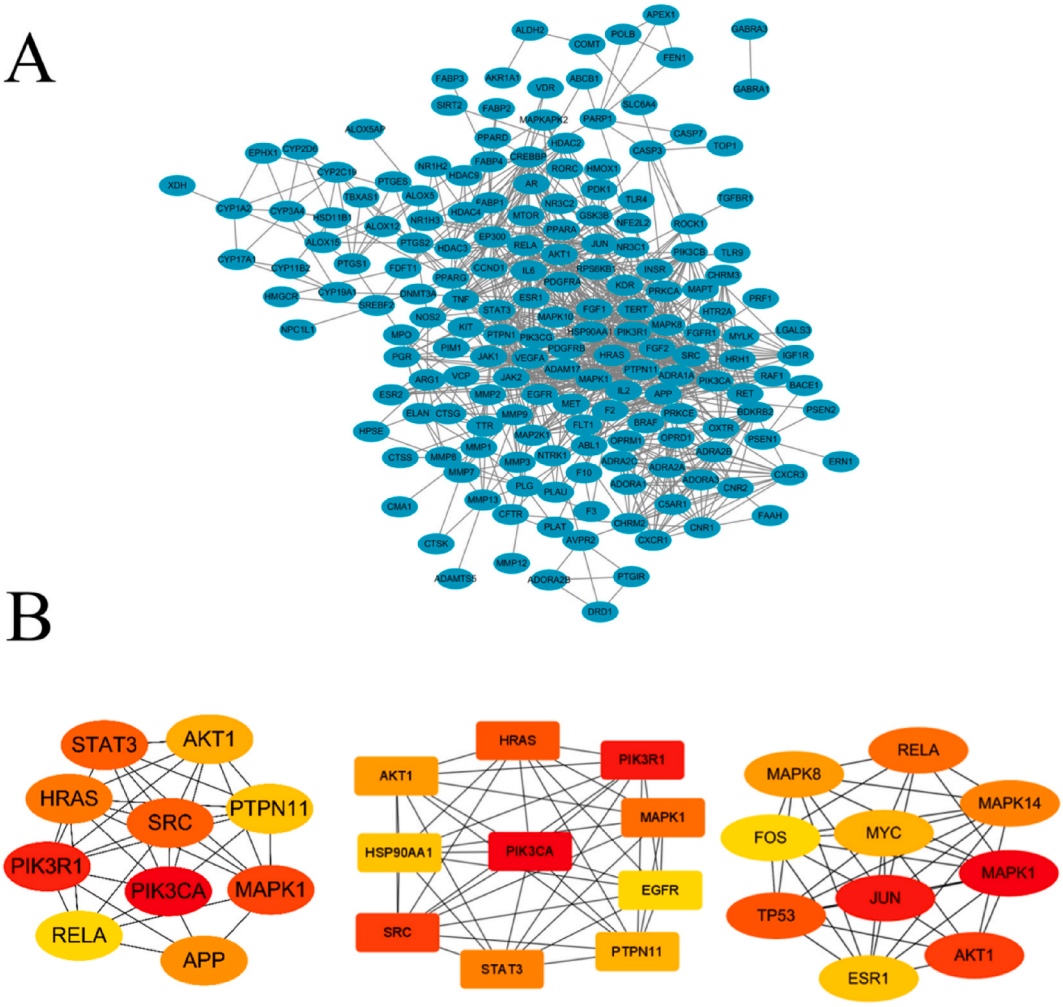

Fig. 3. Diagram of protein–protein interaction network.
(A) Protein-protein interaction network. (B) The top 10 target proteins screened by CytoHubba.

Table 2
Modules of the protein–protein interaction network of common targets of DBD and MI.

Cluster NO.	Targets	MCODE score	Nodes	Edges
1	APP, CNR1, EDNRA, SSTR2, F2R, AGTR1, F2, CASR, ADORA1, KISS1R, GNRHR, CCR3, CXCR3, CXCR2, CXCR1, CXCR4, DRD2, ADORA3, GRM1, EDNRB, CCKBR, NTSR1, ACKR3, CCR1, CCR5, CCR2,	15.12	26	189
2	EPHA3, EPHA4, JAK2, LCK, EPHA7, KAT2B, GRB2, EGFR, RARB, NCOR1, RARA, RXRA, HDAC9, EPHB2, HDAC5, JAK1, IL6, NCOR2, MAPK3, HDAC3, HDAC4, HDAC1, EPHA5, EZH2, HDAC2, HDAC2, RARG, EPHA2, EPHA1, PIK3CB, HDAC6	9.59	30	139
3	MAPK8, JAK3, STAT3, PLK1, NEK2, PTK2, BTK, FGFR3, PPARG, HSP90B1, KIT, SYK, GSNK1D, FLT4, CCND1, IGFBP5, FKBP5, AURKA, BMP4, PRKACA, FLT1, IGFBP1, IGFBP4, PTPN11, PLK4, IGFBP3, MAPK1, PRKCA	6.78	37	122

resistance" (hsa04931), "Relaxin signaling pathway" (hsa04926), and "Calcium signaling pathway" (hsa04020) (Fig. 4A and B). We obtained 831 GO terms across the three categories of BP, CC, and MF (Fig. 4C shows a bubble chart of the top 10 GO terms). For KEGG enrichment analysis, the top 20 pathways out of 164 included: EGFR tyrosine kinases inhibitor resistance, Prostate cancer, Proteoglycans in cancer, and Endocrine resistance, among others (the bar graph of the top 20 is shown in Fig. 4D). These data suggested that the top five signaling pathways closely associated with the treatment of MI with DBD were HIF-1, prolactin, ErbB, Rap1, and PI3K/AKT (the enrichment of genes in the PI3K/AKT signaling pathway is shown in Fig. 4E).

Table 3
Top 10 proteins of Degree, Betweenness, Closeness, and Maximal Clique Centrality (MCC).

Degree		Betweenness		Closeness		Maximal Clique Centrality	
Node_Name	Values	Node_Name	Values	Node_Name	Values	Node_Name	Values
PIK3CA	46	APP	4404.95909	MAPK1	98.65	APP	87178654124
PIK3R1	44	STAT3	3832.12738	PIK3CA	98.65	BDKRB2	87178654080
MAPK1	41	MAPK1	2963.23322	STAT3	98.53	ADRA2C	87178291224
STAT3	38	PTGS2	2809.24863	PIK3R1	97.65	ADRA2B	87178291224
SRC	38	CREBBP	2560.84530	SRC	94.65	ADRA2A	87178291224
HRAS	35	VEGFA	2103.36034	APP	93.40	CHRM2	87178291206
APP	34	PIK3CA	1951.09663	VEGFA	92.28	CNR1	87178291202
AKT1	30	PIK3R1	1822.05970	RELA	91.15	OPRM1	87178291202
PTPN11	28	RELA	1768.43656	HRAS	90.02	CNR2	87178291202
RELA	27	EGFR	1723.62621	AKT1	89.98	OPRD1	87178291202

3.2. Molecular docking to verify active compounds in DBD

The six active compounds in DBD, namely, quercetin, kaempferol, isoflavone, isorhamnetin, hederagenin, and formononetin, had a high binding affinity (Vina score < -5.0) to AKT1, ERK2, and CASPASE-9, as per the CB-dock molecular docking system. A Vina score of $<$ -5.0 is supposed to indicate good binding energy with the target protein [40]. The lowest Vina score for each active compound binding structure image is illustrated in Fig. 5 (A-R).

3.3. Qualitative analysis of DBD

The UPLC chromatogram of mixed standard compounds and DBD is shown in Fig. 6 (A, B). Five authentic reference substances were detected in DBD within 12 min: (1) Calycosin-7-O-β-D-glucoside, (2) Ferulic acid, (3) Calycosin, (4) Formononetin, and (5) Z-Ligustilide.

The chromatograms of (A) standard compounds and (B) DBD. (1) Calycosin-7-O-β-D-glucoside, (2) Ferulic acid, (3) Calycosin, (4) Formononetin, (5) Z-Ligustilide.

3.4. DBD protects against MI pathological changes in the rat model

The TTC staining results showed that intragastric administration of DBD (10 g/kg/d) for one week significantly reduced the infarct size compared with the MI group ($p < 0.01$ versus the MI group, Fig. 7A). Furthermore, H&E staining revealed irregularly distributed myocardial cells, a smaller nucleus, hyperplastic fibrous connective tissues, and inflammatory factor infiltration in the model rat heart tissues, which were relieved by DBD (Fig. 7B). DBD dramatically decreased MI-induced apoptosis in cardiomyocytes, according to the results of the TUNEL staining assay (Fig. 7C).

3.5. DBD treatment regulated the expression of core proteins AKT1, ERK2, and CASPASE-9

Western blotting and immunofluorescence were used to verify the effectiveness of DBD treatment for the core proteins AKT1, ERK2, and CASPASE-9. DBD significantly elevated the AKT1 (Fig. 8A(a), B(a)) and ERK2 (Fig. 8A(b), B(b)) protein levels and reduced the CASPASE-9 (Fig. 8A(c), B(c)) protein level, compared to the MI group.

4. Discussion

To our knowledge, this is the first study to explore overlapping genes of MI with the potential active compounds of DBD. In all, 213 candidate targets were obtained, followed by the PPI network and core target construction, and seven core targets, namely PIK3R1, MAPK1, SRC, STAT3, HRAS, AKT1, and PTPN11 were identified. According to the GO and KEGG pathway enrichment analysis, the PI3K/AKT1 signaling pathway was selected as the key pathway, because of the higher gene ratio and q value. Furthermore, MAP kinases, also called extracellular signal-regulated kinases (ERKs), protect from MI and inflammatory reaction and activate cardiomyocyte regeneration [43,44]. Evidence from previous studies have shown that PI3K/AKT1 and ERKs are linked with MI [45,46]. The activation of PI3K/AKT can inhibit cell death and improve the survival of cardiomyocytes [47]. Furthermore, the downregulation of ERK2 signaling can protect against myocardial ischemic injury *in vivo* and may contribute to cardiomyocyte apoptosis [48]. Hence, AKT1 and ERK2 are the key proteins involved in cardiomyocyte proliferation and apoptosis [49,50]. The validated genes of DBD with MI were selected based on the core gene targets and PI3K/AKT signaling pathway. The validation results indicated that DBD could significantly affect MI through the PI3K/AKT signaling pathway. CASPASE-9, a key signaling molecule associated with PI3K/AKT and ERK2 signaling pathways, demonstrating the apoptotic change in infarct cardiomyocytes' mitochondria [51]. Validation results also demonstrated that DBD decreased the elevation of CASPASE-9 levels in the MI model.

Based on bioinformatics database research, our study systematically elucidated the active compounds of DBD. From a mechanistic point of view, by applying network pharmacology methods, our study provided a potentially novel signaling mechanism of action of

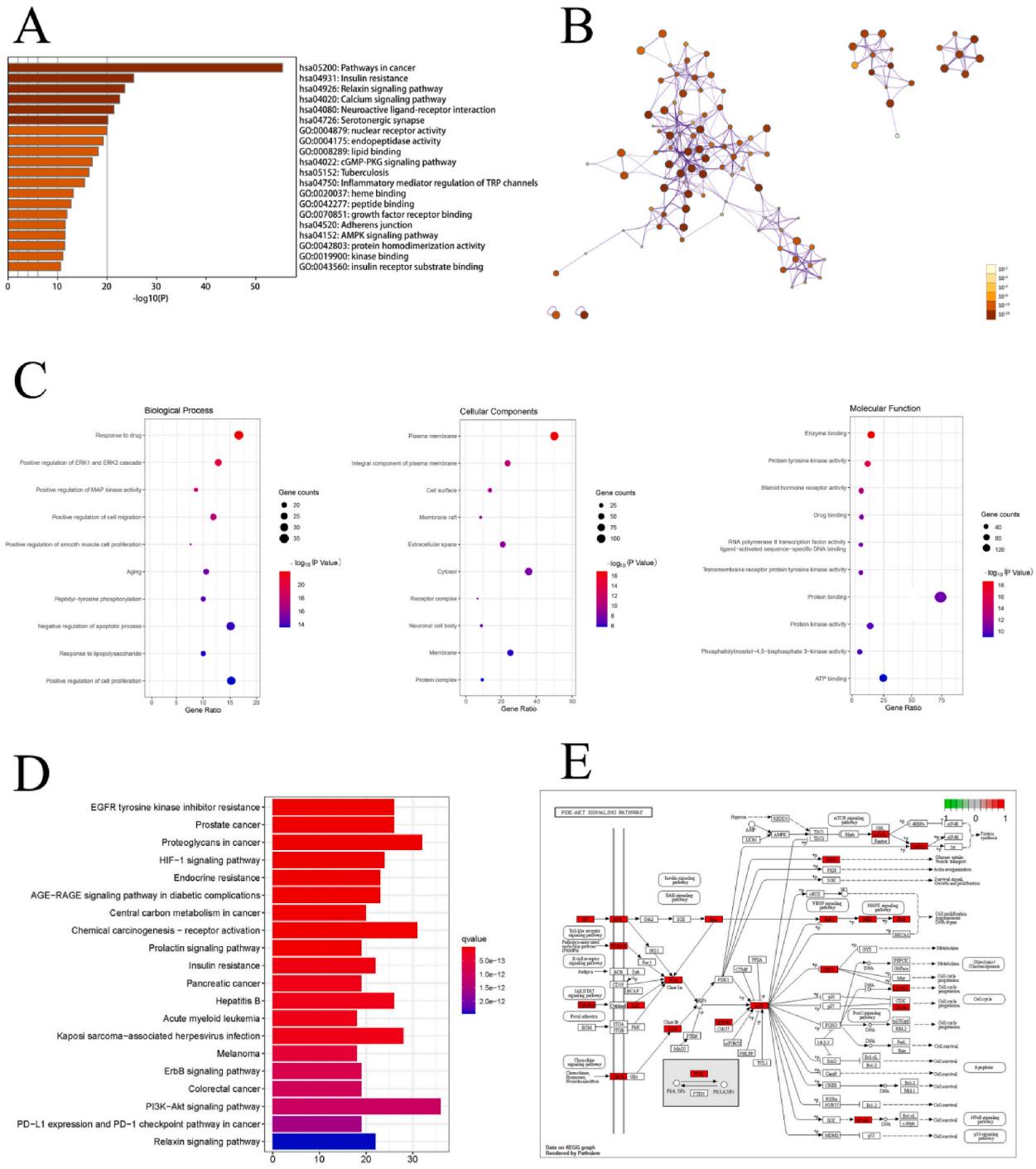

Fig. 4. The critical pathways screened by network pharmacology.
(A–B) Functional enrichment analysis of target genes using Metascape. (C) GO enrichment analysis. (D) Analysis of KEGG pathway enrichment. (E) The PI3K/AKT signaling pathway.

DBD against MI. We searched for potential active compounds from the TCMSP (OB $\geq$ 30 % and DL $\geq$ 0.18) and potential active compounds, namely astragaloside II, astragaloside III, astragaloside IV, calycosin-7-O-β-D-glucoside, stigmasterol, and ferulic acid in the literature [14,26,52]. Six core active chemical compounds in DBD were noted based on the compound-target network. These compounds include quercetin, kaempferol, isoflavanone, isorhamnetin, hederagenin, and formononetin. Quercetin, a common flavonoid, has anti-oxidant, anti-inflammatory, anti-ischemic, and anti-apoptotic functions to provide cardioprotective effects [53]. A

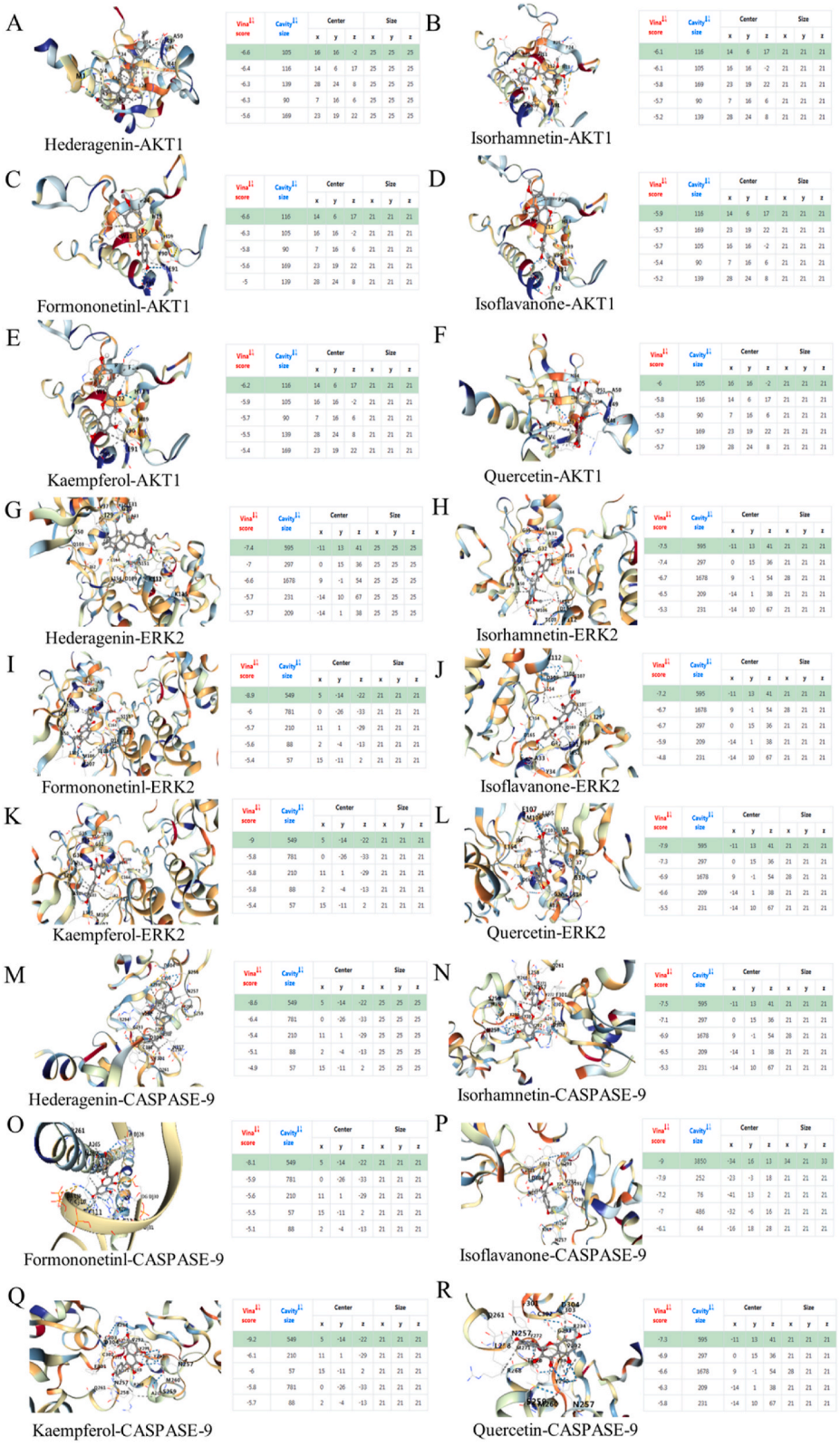

Fig. 5. (A–R) CB-Dock validation of quercetin, kaempferol, isoflavanone, isorhamnetin, hederagenin, and formononetin binding with AKT1, ERK2, and CASPASE-9.

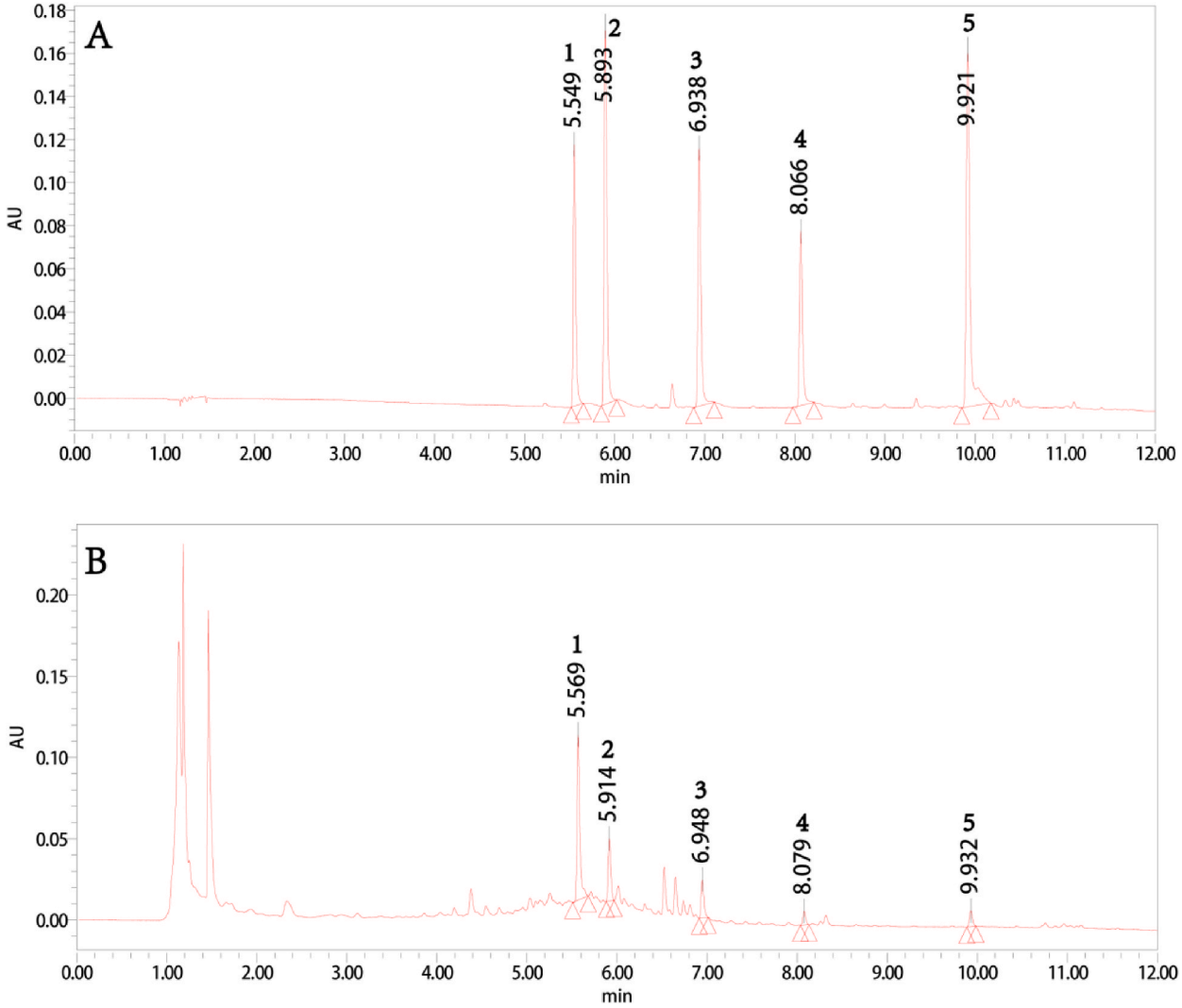

Fig. 6. UPLC-PDA analysis of DBD.

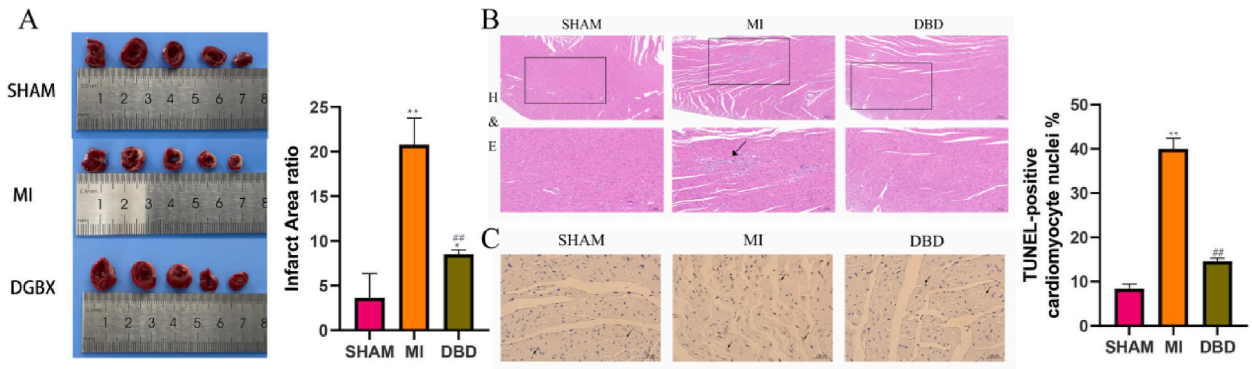

Fig. 7. DBD protects against MI pathological changes in rat model.
(A) DBD alleviates the infarct ratio in MI rat model. (B) Histopathological changes in MI rat model treated with DBD (original magnifications, 50 × and 100 × , inflammation cells: black arrow). (C) TUNEL assay in MI rat model treated with DBD (original magnifications: 400 × , TUNEL-positive: black arrow). Data are presented as the mean ± SD (n = 3). $^{**}p < 0.01$ versus the sham group; $^{\#\#}p < 0.01$ versus the MI group.

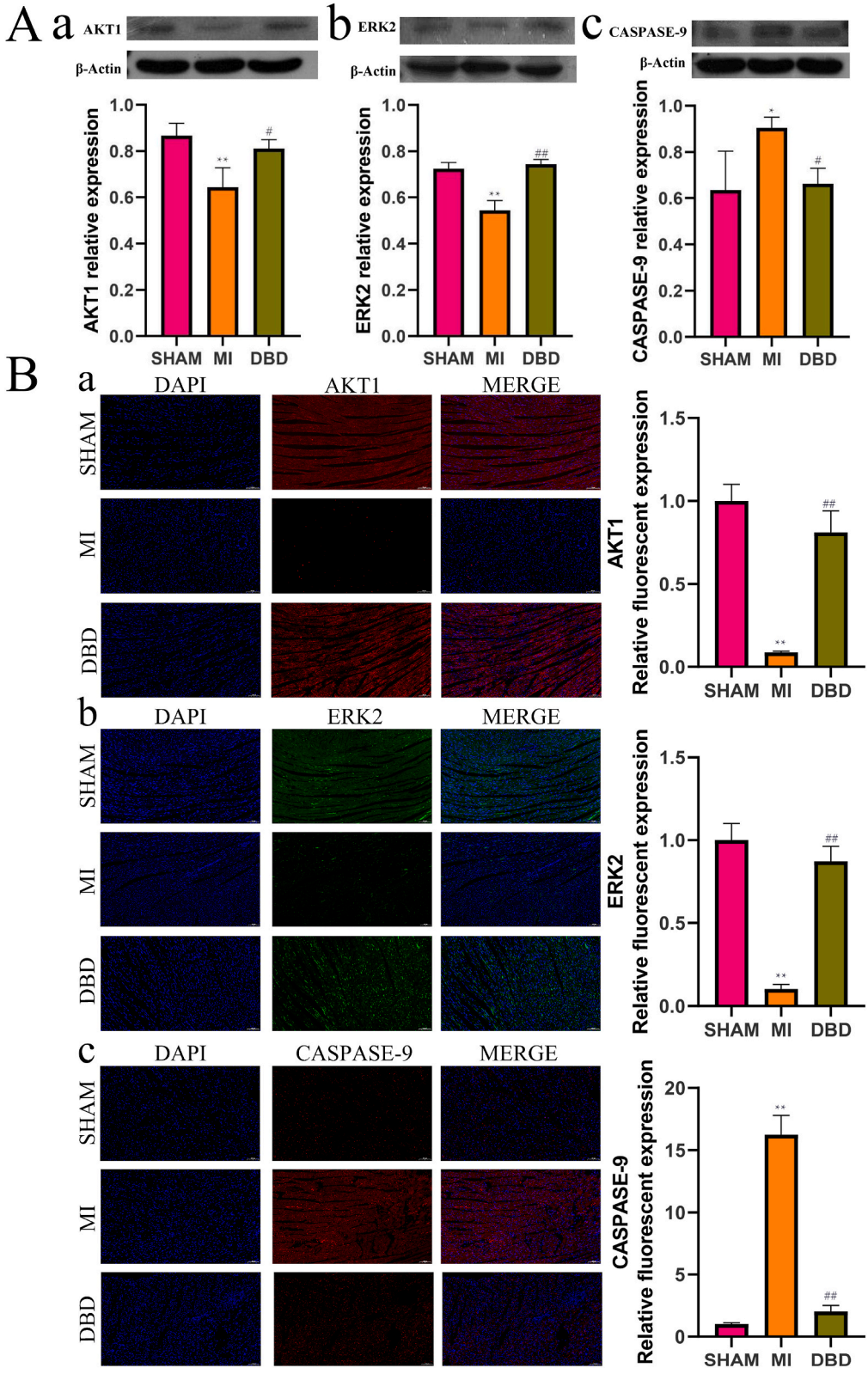

(caption on next page)

Fig. 8. The expression of core proteins AKT1, ERK2, and CASPASE-9.
(A) Relative protein expression levels of AKT1 (a), ERK2 (b), and CASPASE-9 (c) treated with DBD in the MI rat model. Data are presented as the mean ± SD (n = 3). $^{*}P < 0.05$ and $^{**}P < 0.01$ versus the sham group; $^{\#}P < 0.05$ and $^{\#\#}P < 0.01$ versus the MI group. (B) Immunofluorescence staining to detect the effect of DBD treatment on core proteins expression (original magnifications: 100 ×). (a–c) The expression of AKT1, ERK2, and CASPASE-9. Data are presented as the mean ± SD (n = 3). $^{**}P < 0.01$ versus the sham group; $^{\#\#}P < 0.01$ versus the MI group.

randomized clinical trial study indicated that post-MI patients who received quercetin 500 mg/day for 8 weeks exhibited enhanced total antioxidant capacity (TAC) in serum compared with the placebo group [49]. In an animal model study, quercetin showed strong evidence of protection against myocardial ischemia and reperfusion injury, whether used as pre-treatment or post-treatment, by inhibiting the NF-κB pathway [54], apoptosis, and oxidative stress [52], as well as by activating the NO system [55] *in vivo*. Quercetin also displayed cardioprotective effects by reducing AKT and ERK levels and enhancing GSK-3 levels in a myocardial hypertrophy model [56]. Kaempferol reduces the lipid profile and protects against MI and oxidative stress [57]. Kaempferol has been proven to reduce MI damage via the MAPK and PI3K/AKT/GSK-3β signaling pathways [58,59]. Isoflavonoids have already been found to lower the risk of coronary heart disease [60]. *In vitro*, isoflavone can reduce symptoms of CVDs by regulating the ERK1/2 and NF-κB pathways [61]. Isorhamnetin prevents cardiac hypertrophy by blocking the PI3K/AKT pathway [62], as well as hypoxia/reoxygenation damage through anti-apoptosis and oxidative stress pathways [63,64]. The use of hederagenin has not been reported in cardioprotection; however, it can inhibit the release of iNOS and promote eNOS synthesis for endothelial function, as shown in an *in vivo* study [65]. Formononetin prevents MI by reducing ROS levels, cardiomyocyte apoptosis, and enhancing autophagic degradation and ATP synthase activation [66–68].

In vivo studies showed that DBD had significant cardioprotective effects against an MI rat model, per the results of TTC staining. The staining results showed a significant elevation of the infarct area ratio in the hearts of MI rats, while treatment with DBD reverted this phenomenon. H&E staining revealed irregularly arranged myocardial cells, smaller nucleus, hyperplastic fibrous connective tissues, and inflammatory factor infiltration in MI rats' heart tissues; DBD therapy reduced cardiomyocyte lesions. Western blot analysis and immunofluorescence assay showed that AKT1 and ERK2 expression was inhibited, while CASPASE-9 was expressed in the MI surgery model. However, treatment with DBD reversed this trend. Our data show a cardioprotective effect of DBD in the MI rat heart, which may be mediated through the PI3K/AKT signaling pathway.

5. Conclusions

Our study analyzed the potential active compounds in DBD with predicted genes overlapping in MI. The biochemical and histological data indicate the cardioprotective benefits of DBD in the context of MI *in vivo*, encouraging further research to investigate the molecular mechanisms of DBD's activity and the feasibility of its application in ischemic heart disease. Although critical proteins in the PI3K/AKT pathway were verified in this investigation, more research is needed in the future to explore the potential involvement of other molecular pathways underlying DBD's cardioprotective effect on MI.

Ethical statement

All animal experiments were carried out following the EEC Directive of 1986 (86/609/EEC) and were approved by the Ethics Committee of the Anhui University of Chinese Medicine (AHUCM-rats-2022008).

Data availability statement

Data included in article/supp. material/referenced in article.

Disclosure statement

The authors declare that the research was conducted in the absence of any commercial or financial relationships that could be construed as a potential conflict of interest.

Funding

This word was supported by the National Natural Science Foundation of China (No. 81904147) and Scientific Research Project for Universities in Anhui Province (No. 2023AH050867).

CRediT authorship contribution statement

Chuqiao Shen: Writing – review & editing, Writing – original draft, Investigation, Funding acquisition, Formal analysis, Conceptualization. **Qian Chen:** Writing – original draft, Investigation. **Shuo Chen:** Writing – review & editing, Methodology, Formal analysis. **Yixuan Lin:** Writing – review & editing, Conceptualization.

Declaration of competing interest

The authors declare that they have no known competing financial interests or personal relationships that could have appeared to influence the work reported in this paper.

Appendix A. Supplementary data

Supplementary data to this article can be found online at https://doi.org/10.1016/j.heliyon.2024.e29360.

References

[1] E. Braunwald, M. Nicholls, Leaders in cardiovascular medicine. Eugene Braunwald, MD: an icon of the 20th century still going strong, Eur. Heart J. 36 (2015) 1350–1351, https://doi.org/10.1093/eurheartj/ehv101.

[2] P.M. Boarescu, I. Chirilă, A.E. Bulboacă, et al., Effects of curcumin nanoparticles in isoproterenol-induced myocardial infarction, Oxid. Med. Cell. Longev. 2019 (2019) 7847142, https://doi.org/10.1155/2019/7847142.

[3] P. Hao, F. Jiang, J. Cheng, L. Ma, Y. Zhang, Y. Zhao, Traditional Chinese medicine for cardiovascular disease: evidence and potential mechanisms, J. Am. Coll. Cardiol. 69 (2017) 2952–2966, https://doi.org/10.1016/j.jacc.2017.04.041.

[4] J.F. Chen, F. Liu, M.M. Qiao, et al., Vasorelaxant effect of curcubisabolanin A isolated from Curcuma longa through the PI3K/Akt/eNOS signaling pathway, J. Ethnopharmacol. 294 (2022) 115332, https://doi.org/10.1016/j.jep.2022.115332.

[5] Y. Jiang, Q. Zhao, L. Li, S. Huang, S. Yi, Z. Hu, Effect of traditional Chinese medicine on the cardiovascular diseases, Front. Pharmacol. 13 (2022) 806300, https://doi.org/10.3389/fphar.2022.806300.

[6] T.T. Dong, K.J. Zhao, Q.T. Gao, et al., Chemical and biological assessment of a Chinese herbal decoction containing Radix Astragali and Radix Angelicae sinensis: determination of drug ratio in having optimized properties, J. Agric. Food Chem. 54 (2006) 2767–2774, https://doi.org/10.1021/jf053163l.

[7] H.Q. Lin, A.G. Gong, H.Y. Wang, et al., Danggui Buxue tang (astragali Radix and angelicae sinensis Radix) for menopausal symptoms: a review, J. Ethnopharmacol. 199 (2017) 205–210, https://doi.org/10.1016/j.jep.2017.01.044.

[8] G. Hu, P. Yang, Y. Zeng, S. Zhang, J. Song, Danggui Buxue decoction promotes angiogenesis by up-regulation of VEGFR1/2 expressions and down-regulation of sVEGFR1/2 expression in myocardial infarction rat, J. Chin. Med. Assoc. 81 (2018) 37–46, https://doi.org/10.1016/j.jcma.2017.06.015.

[9] K. Liu, X.M. Ren, Q.S. You, et al., Ameliorative effect of Dangguibuxue decoction against cyclophosphamide-induced heart injury in mice, BioMed Res. Int. 2018 (2018) 8503109, https://doi.org/10.1155/2018/8503109.

[10] H. Bo, J. He, X. Wang, et al., Danggui Buxue Tang promotes the adhesion and migration of bone marrow stromal cells via the focal adhesion pathway in vitro, J. Ethnopharmacol. 231 (2019) 90–97, https://doi.org/10.1016/j.jep.2018.11.018.

[11] Y. Liu, M. Chang, Z. Hu, et al., Danggui Buxue decoction enhances the anticancer activity of gemcitabine and alleviates gemcitabine-induced myelosuppression, J. Ethnopharmacol. 273 (2021) 113965, https://doi.org/10.1016/j.jep.2021.113965.

[12] Y. Liu, Z. Wang, X. Qin, Metabolomics and molecular docking to compare of the efficacies of wild-simulated and transplanted Astragali Radix based on its compatibility with Angelicae sinensis Radix against blood deficiency, J. Chromatogr., B: Anal. Technol. Biomed. Life Sci. 1173 (2021) 122682, https://doi.org/10.1016/j.jchromb.2021.122682.

[13] A.G. Gong, V.Y. Huang, H.Y. Wang, H.Q. Lin, T.T. Dong, K.W. Tsim, Ferulic acid orchestrates anti-oxidative properties of Danggui Buxue Tang, an ancient herbal decoction: elucidation by chemical knock-out approach, PLoS One 11 (2016) e0165486, https://doi.org/10.1371/journal.pone.0165486.

[14] K.K.L. Kwan, Y. Huang, K.W. Leung, T.T.X. Dong, K.W.K. Tsim, Danggui Buxue Tang, a Chinese herbal decoction containing astragali Radix and angelicae sinensis Radix, modulates mitochondrial bioenergetics in cultured cardiomyoblasts, Front. Pharmacol. 10 (2019) 614, https://doi.org/10.3389/fphar.2019.00614.

[15] C. Li, F. Zhu, S. Wang, J. Wang, B. Wu, Danggui Buxue decoction ameliorates inflammatory bowel disease by improving inflammation and rebuilding intestinal mucosal barrier, Evid. Based Complement. Alternat. Med. 2021 (2021) 8853141, https://doi.org/10.1155/2021/8853141.

[16] J. Liu, J. Wei, C. Wang, et al., The combination of Radix Astragali and Radix Angelicae sinensis attenuates the IFN-gamma-induced immune destruction of hematopoiesis in bone marrow cells, BMC Compl. Alternative Med. 19 (2019) 356, https://doi.org/10.1186/s12906-019-2781-4.

[17] Y. Shen, B. Zhang, X. Pang, et al., Network pharmacology-based analysis of Xiao-Xu-Ming decoction on the treatment of Alzheimer's disease, Front. Pharmacol. 11 (2020) 595254, https://doi.org/10.3389/fphar.2020.595254.

[18] P.K. Kumar Pasala, M. Donakonda, P.S.N.B.K. Dintakurthi, M. Rudrapal, S.A. Gouru, K. Ruksana, Investigation of cardioprotective activity of silybin: network pharmacology, molecular docking, and in vivo studies, ChemistrySelect 8 (2023), https://doi.org/10.1002/slct.202300148.

[19] M. Kibble, N. Saarinen, J. Tang, K. Wennerberg, S. Mäkelä, T. Aittokallio, Network pharmacology applications to map the unexplored target space and therapeutic potential of natural products, Nat. Prod. Rep. 32 (2015) 1249–1266, https://doi.org/10.1039/c5np00005j.

[20] J.A. Ezugwu, U.C. Okoro, M.A. Ezeokonkwo, et al., Design, synthesis, molecular docking, molecular dynamics and in vivo antimalarial activity of new dipeptide-sulfonamides, ChemistrySelect 7 (2022), https://doi.org/10.1002/slct.202103908.

[21] A.R. Issahaku, E.Y. Salifu, C. Agoni, et al., Discovery of potential KRAS-SOS1 inhibitors from South African natural compounds: an in silico approach, ChemistrySelect 8 (2023), https://doi.org/10.1002/slct.202300277.

[22] J. Ru, P. Li, J. Wang, et al., TCMSP: a database of systems pharmacology for drug discovery from herbal medicines, J. Cheminf. 6 (2014) 13, https://doi.org/10.1186/1758-2946-6-13.

[23] I.M.M. Othman, M.H. Mahross, M.A.M. Gad-Elkareem, et al., Toward a treatment of antibacterial and antifungal infections: design, synthesis and in vitro activity of novel arylhydrazothiazolylsulfonamides analogues and their insight of DFT, docking and molecular dynamic simulations, J. Mol. Struct. 1243 (2021), https://doi.org/10.1016/j.molstruc.2021.130862.

[24] R. Baru Venkata, D.S.N.B.K. Prasanth, P.K. Pasala, et al., Utilizing Andrographis paniculata leaves and roots by effective usage of the bioactive andrographolide and its nanodelivery: investigation of antikindling and antioxidant activities through in silico and in vivo studies, Front. Nutr. 10 (2023) 1185236, https://doi.org/10.3389/fnut.2023.1185236.

[25] M. Rudrapal, W.A. Eltayeb, G. Rakshit, et al., Dual synergistic inhibition of COX and LOX by potential chemicals from Indian daily spices investigated through detailed computational studies, Sci. Rep. 13 (2023) 8656, https://doi.org/10.1038/s41598-023-35161-0.

[26] L.P. Zhou, K.Y. Wong, H.T. Yeung, et al., Bone protective effects of Danggui Buxue Tang alone and in combination with tamoxifen or raloxifene in vivo and in vitro, Front. Pharmacol. 9 (2018) 779, https://doi.org/10.3389/fphar.2018.00779.

[27] G. Stelzer, N. Rosen, I. Plaschkes, et al., The GeneCards suite: from gene data mining to disease genome sequence analyses, Curr. Protoc. Bioinformatics 54 (2016) 33, https://doi.org/10.1002/cpbi.5.

[28] J.S. Amberger, A. Hamosh, Searching online mendelian inheritance in man (OMIM): a KnowledgeBase of human genes and genetic phenotypes, Curr. Protoc. Bioinformatics 58 (1.2.1–1.2.12) (2017), https://doi.org/10.1002/cpbi.27.

[29] A. Daina, O. Michielin, V. Zoete, SwissTargetPrediction: updated data and new features for efficient prediction of protein targets of small molecules, Nucleic Acids Res. 47 (2019) W357–W364, https://doi.org/10.1093/nar/gkz382.

[30] UniProt Consortium, UniProt: the universal protein KnowledgeBase in 2021, Nucleic Acids Res. 49 (2021) D480–D489, https://doi.org/10.1093/nar/gkaa1100.
[31] P. Shannon, A. Markiel, O. Ozier, et al., Cytoscape: a software environment for integrated models of biomolecular interaction networks, Genome Res. 13 (2003) 2498–2504, https://doi.org/10.1101/gr.1239303.
[32] D. Szklarczyk, A.L. Gable, K.C. Nastou, et al., The STRING database in 2021: customizable protein-protein networks, and functional characterization of user-uploaded gene/measurement sets, Nucleic Acids Res. 49 (2021) D605–D612, https://doi.org/10.1093/nar/gkaa1074.
[33] C.H. Chin, S.H. Chen, H.H. Wu, C.W. Ho, M.T. Ko, C.Y. Lin, cytoHubba: identifying hub objects and sub-networks from complex interactome, BMC Syst. Biol. 8 (2014) S11, https://doi.org/10.1186/1752-0509-8-S4-S11.
[34] R. Saito, M.E. Smoot, K. Ono, et al., A travel guide to cytoscape plugins, Nat. Methods 9 (2012) 1069–1076, https://doi.org/10.1038/nmeth.2212.
[35] X. Jiao, B.T. Sherman, W. da Huang, et al., David-WS: a stateful web service to facilitate gene/protein list analysis, Bioinformatics 28 (2012) 1805–1806, https://doi.org/10.1093/bioinformatics/bts251.
[36] M. Kanehisa, M. Furumichi, M. Tanabe, Y. Sato, K. Morishima, KEGG: new perspectives on genomes, pathways, diseases and drugs, Nucleic Acids Res. 45 (2017) D353–D361, https://doi.org/10.1093/nar/gkw1092.
[37] L. Pinzi, G. Rastelli, Molecular docking: shifting paradigms in drug discovery, Int. J. Mol. Sci. 20 (2019), https://doi.org/10.3390/ijms20184331.
[38] Y. Liu, M. Grimm, W.T. Dai, M.C. Hou, Z.X. Xiao, Y. Cao, CB-Dock: a web server for cavity detection-guided protein-ligand blind docking, Acta Pharmacol. Sin. 41 (2020) 138–144, https://doi.org/10.1038/s41401-019-0228-6.
[39] Y. Li, S. Guo, Y. Zhu, et al., Flowers of Astragalus membranaceus var mongholicus as a novel high potential by-product: phytochemical characterization and antioxidant activity, Molecules 24 (2019), https://doi.org/10.3390/molecules24030434.
[40] A. Labed, M. Ferhat, I. Labed-Zouad, et al., Compounds from the pods of Astragalus armatus with antioxidant, anticholinesterase, antibacterial and phagocytic activities, Pharm. Biol. 54 (2016) 3026–3032, https://doi.org/10.1080/13880209.2016.1200632.
[41] F. Liu, L. Sun, G. You, H. Liu, X. Ren, M. Wang, Effects of Astragalus polysaccharide on the solubility and stability of 15 flavonoids, Int. J. Biol. Macromol. 143 (2020) 873–880, https://doi.org/10.1016/j.ijbiomac.2019.09.148.
[42] L.W. Qi, J. Cao, P. Li, Y.X. Wang, Rapid and sensitive quantitation of major constituents in Danggui Buxue Tang by ultra-fast HPLC-TOF/MS, J. Pharm. Biomed. Anal. 49 (2009) 502–507, https://doi.org/10.1016/j.jpba.2008.10.026.
[43] E. Bassat, Y.E. Mutlak, A. Genzelinakh, et al., The extracellular matrix protein agrin promotes heart regeneration in mice, Nature 547 (2017) 179–184, https://doi.org/10.1038/nature22978.
[44] H. Xu, M. Liu, G. Chen, et al., Anti-inflammatory effects of ginsenoside Rb3 in LPS-induced macrophages through direct inhibition of TLR4 signaling pathway, Front. Pharmacol. 13 (2022) 714554, https://doi.org/10.3389/fphar.2022.714554.
[45] T. Matsui, J. Tao, F. del Monte, et al., Akt activation preserves cardiac function and prevents injury after transient cardiac ischemia in vivo, Circulation 104 (2001) 330–335, https://doi.org/10.1161/01.cir.104.3.330.
[46] M. Abbas, L. Jesel, C. Auger, et al., Endothelial microparticles from acute coronary syndrome patients induce premature coronary artery endothelial cell aging and thrombogenicity: role of the Ang II/AT1 receptor/NADPH oxidase-mediated activation of MAPKs and PI3-kinase pathways, Circulation 135 (2017) 280–296, https://doi.org/10.1161/CIRCULATIONAHA.116.017513.
[47] E. Chen, C. Chen, Z. Niu, et al., Poly(I:C) preconditioning protects the heart against myocardial ischemia/reperfusion injury through TLR3/PI3K/Akt-dependent pathway, Signal Transduct. Target. Ther. 5 (2020) 216, https://doi.org/10.1038/s41392-020-00257-w.
[48] D. Zhang, L. Zhu, C. Li, et al., Sialyltransferase7A, a Klf4-responsive gene, promotes cardiomyocyte apoptosis during myocardial infarction, Basic Res. Cardiol. 110 (2015) 28, https://doi.org/10.1007/s00395-015-0484-7.
[49] H. Okumura, N. Nagaya, T. Itoh, et al., Adrenomedullin infusion attenuates myocardial ischemia/reperfusion injury through the phosphatidylinositol 3-kinase/Akt-dependent pathway, Circulation 109 (2004) 242–248, https://doi.org/10.1161/01.CIR.0000109214.30211.7C.
[50] S. Garg, S.I. Khan, R.K. Malhotra, et al., The molecular mechanism involved in cardioprotection by the dietary flavonoid fisetin as an agonist of PPAR-γ in a murine model of myocardial infarction, Arch. Biochem. Biophys. 694 (2020) 108572, https://doi.org/10.1016/j.abb.2020.108572.
[51] Y. Zhang, Y. Wang, J. Xu, et al., Melatonin attenuates myocardial ischemia-reperfusion injury via improving mitochondrial fusion/mitophagy and activating the AMPK-OPA1 signaling pathways, J. Pineal Res. 66 (2019) e12542, https://doi.org/10.1111/jpi.12542.
[52] C.J. Liu, L. Yao, Y.M. Hu, B.T. Zhao, Effect of quercetin-loaded mesoporous silica nanoparticles on myocardial ischemia-reperfusion injury in rats and its mechanism, Int. J. Nanomedicine 16 (2021) 741–752, https://doi.org/10.2147/IJN.S277377.
[53] K. Ferenczyova, B. Kalocayova, M. Bartekova, Potential implications of quercetin and its derivatives in cardioprotection, Int. J. Mol. Sci. 21 (2020), https://doi.org/10.3390/ijms21051585.
[54] M. Kumar, E.R. Kasala, L.N. Bodduluru, V. Kumar, M. Lahkar, Molecular and biochemical evidence on the protective effects of quercetin in isoproterenol-induced acute myocardial injury in rats, J. Biochem. Mol. Toxicol. 31 (2017) 1–8, https://doi.org/10.1002/jbt.21832.
[55] Y. Liu, Y. Song, S. Li, L. Mo, Cardioprotective effect of quercetin against ischemia/reperfusion injury is mediated through NO system and mitochondrial K-ATP channels, Cell J 23 (2021) 184–190, https://doi.org/10.22074/cellj.2021.7183.
[56] K. Chen, M. Rekep, W. Wei, et al., Quercetin prevents in vivo and in vitro myocardial hypertrophy through the proteasome-GSK-3 pathway, Cardiovasc. Drugs Ther. 32 (2018) 5–21, https://doi.org/10.1007/s10557-018-6771-4.
[57] A. Vishwakarma, T.U. Singh, S. Rungsung, et al., Effect of kaempferol pretreatment on myocardial injury in rats, Cardiovasc. Toxicol. 18 (2018) 312–328, https://doi.org/10.1007/s12012-018-9443-5.
[58] K. Suchal, S. Malik, N. Gamad, et al., Kaempferol attenuates myocardial ischemic injury via inhibition of MAPK signaling pathway in experimental model of myocardial ischemia-reperfusion injury, Oxid. Med. Cell. Longev. 2016 (2016) 7580731, https://doi.org/10.1155/2016/7580731.
[59] L. Zhang, Z. Guo, Y. Wang, J. Geng, S. Han, The protective effect of kaempferol on heart via the regulation of Nrf2, NF-κβ, and PI3K/Akt/GSK-3β signaling pathways in isoproterenol-induced heart failure in diabetic rats, Drug Dev. Res. 80 (2019) 294–309, https://doi.org/10.1002/ddr.21495.
[60] X. Zhang, Y.T. Gao, G. Yang, et al., Urinary isoflavonoids and risk of coronary heart disease, Int. J. Epidemiol. 41 (2012) 1367–1375, https://doi.org/10.1093/ije/dys130.
[61] C. Borrás, J. Gambini, M.C. Gómez-Cabrera, et al., Genistein, a soy isoflavone, up-regulates expression of antioxidant genes: involvement of estrogen receptors, ERK1/2, and NFkappaB, Faseb. J. 20 (2006) 2136–2138, https://doi.org/10.1096/fj.05-5522fje.
[62] L. Gao, R. Yao, Y. Liu, et al., Isorhamnetin protects against cardiac hypertrophy through blocking PI3K-AKT pathway, Mol. Cell. Biochem. 429 (2017) 167–177, https://doi.org/10.1007/s11010-017-2944-x.
[63] T.T. Zhao, T.L. Yang, L. Gong, P. Wu, Isorhamnetin protects against hypoxia/reoxygenation-induced injure by attenuating apoptosis and oxidative stress in H9c2 cardiomyocytes, Gene 666 (2018) 92–99, https://doi.org/10.1016/j.gene.2018.05.009.
[64] Y. Xu, C. Tang, S. Tan, J. Duan, H. Tian, Y. Yang, Cardioprotective effect of isorhamnetin against myocardial ischemia reperfusion (I/R) injury in isolated rat heart through attenuation of apoptosis, J. Cell Mol. Med. 24 (2020) 6253–6262, https://doi.org/10.1111/jcmm.15267.
[65] S.H. Lu, J.H. Guan, Y.L. Huang, et al., Experimental study of antiatherosclerosis effects with hederagenin in rats, Evid. Based Complement. Alternat. Med. 2015 (2015) 456354, https://doi.org/10.1155/2015/456354.
[66] S. Zhang, X. Tang, J. Tian, et al., Cardioprotective effect of sulphonated formononetin on acute myocardial infarction in rats, Basic Clin. Pharmacol. Toxicol. 108 (2011) 390–395, https://doi.org/10.1111/j.1742-7843.2011.00676.x.
[67] Z. Huang, Y. Liu, X. Huang, Formononetin may protect aged hearts from ischemia/reperfusion damage by enhancing autophagic degradation, Mol. Med. Rep. 18 (2018) 4821–4830, https://doi.org/10.3892/mmr.2018.9544.
[68] D.S. Wang, L.Y. Yan, D.Z. Yang, et al., Formononetin ameliorates myocardial ischemia/reperfusion injury in rats by suppressing the ROS-TXNIP-NLRP3 pathway, Biochem. Biophys. Res. Commun. 525 (2020) 759–766, https://doi.org/10.1016/j.bbrc.2020.02.147.